Journal of Physics: Conference Series **465** (2013) 012006 doi:10.1088/1742-6596/465/1/012006

Re-entry dynamics of high area-to-mass ratio objects in eccentric Earth orbits considering drag and solar radiation pressure

E Bauer Espitia[1] and W Schulz[2]

Orbital Dynamics Group – ODin, Dep. Aeronáutica, FCEFyN, Universidad Nacional de Córdoba – UNC, Argentina

[1] eloybauer@gmail.com
[2] wschulz@efn.uncor.edu

Abstract. The discovery of a new population of objects with high area-to-mass ratios (HAMR) in orbits near the geostationary ring has motivated recent research seeking to understand the behaviour of those debris under the influence of certain types of disturbances, such as solar radiation pressure and atmospheric drag. Based on a series of selection criteria, it was made from the NORAD catalogue a list of potential candidates for study. As we developed an orbital propagator that takes into account the major disturbances, it was possible to study the behaviour and variation of orbital parameters during decay of the HAMR objects. The results obtained for two cases studied exhibit the dynamic behaviour of all orbital parameters and show good agreement with the observed decay times.

1. Introduction

Recent research on the population of artificial objects orbiting the Earth revealed a considerable amount of space debris at high altitudes in the range of dimensions of 10 cm to 1 m [1]. The discovery of these objects with traits in the geostationary transfer area was unexpected in a population where in principle there are no potential progenitors. The orbital periods of these objects are about one revolution per day and their eccentricities are distributed between 0 and 0.6. The most significant characteristic of this new class of debris is that they have area-to-mass ratio so high that are several orders of magnitude larger than those of the "normal" space debris previously cataloged [2]. In turn this supports the hypothesis that the new population corresponds to the debris generated at or near the geostationary ring and are in orbits with varying eccentricities due to disturbances of solar radiation pressure [2].

This work aims to study the dynamics of the high area-to-mass ratio objects (HAMR) not only subject to solar radiation pressure (SRP) as also the air drag in its possible passage through the atmosphere. In this first step, we use the model of cannonball for the SRP and the International Standard Atmosphere to determine the density of the atmosphere at different altitudes into account. In future works the Earth's non-homogeneous gravitational potential will be taken into account and the results will be compared with more accurate models like the ones from Scheeres [3, 4].

2. Equations of motion

Based on an inertial reference system centered on earth we use the following equations to describe the dynamical behavior of HAMR objects [5]:

$$[a]_I = \frac{1}{m_S}[F]_I \tag{1}$$

$$[F]_I = [F]_G + [F]_{SRP} + [F]_D \tag{2}$$

Here $[a]_I$ is the acceleration vector, m_S the spacecraft mass, $[F]_I$ the resultant force vector, $[F]_G$ the gravitational force one, $[F]_{SRP}$ the resultant solar radiation pressure vector and $[F]_D$ the drag force one. See Figure 1.

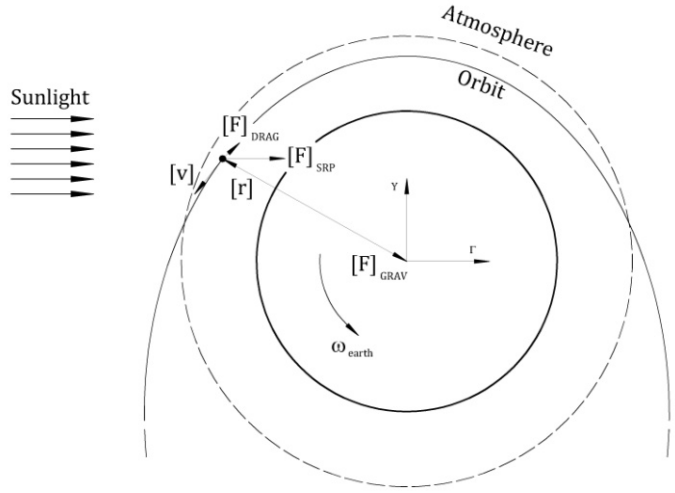

Fig. 1 – Vectorial scheme of forces over HAMR objects.

Additionally:

$$[F]_G = m_S \nabla \frac{GM_\oplus}{r} \sum_{n=0}^{\infty} \sum_{m=0}^{n} \frac{R_\oplus^n}{r^n} P_{nm}(\sin\phi)\left\{C_{nm}\cos(m\lambda) + S_{nm}\sin(m\lambda)\right\} \tag{3}$$

For the geopotential we used G for the universal gravitational constant, $M_\oplus$ for the Earth's mass and $R_\oplus$ for its radio. r is the magnitude of the distance between the satellite and the center of the Earth, P_{nm} are the associated Legendre polynomials of degree n and order m, while C_{nm} and S_{nm} stands for the coefficients that describe the dependence on Earth's internal mass distribution. The geocentric latitude is ϕ and the longitude is λ.

$$[F]_{SRP} = \frac{A(1+\rho_S)P_\Phi}{d^2}\hat{d} \tag{4}$$

The solar radiation pressure model considers A the cross-section area normal to the solar flux, ρ_S the reflectivity, $P_\odot$ the solar radiation pressure that is constant and $[d]$ the Sun-satellite vector.

$$[F]_D = -\frac{1}{2}\rho C_D A v_r^2 \hat{\mathbf{e}}_\mathbf{v} \tag{5}$$

While for the drag force ρ is the atmospheric density, the drag coefficient, C_D, is a dimensionless quantity that describes the interaction of the atmosphere with the satellite's material, v_r is the velocity of the vehicle relative to the air and $\hat{\mathbf{e}}_v$ defines the direction of the relative velocity vector.

3. HAMR objects

In order to simulate the dynamical evolution, some special cases were selected based on a set of semi-major axis, eccentricity and area-to-mass ratios according with HAMR debris characteristics. The initial conditions for the tested cases, given in terms of mean Keplerian orbital elements, are provided in Table 1.

NORAD Number	a [km]	e	i [°]	Ω [°]	ω [°]	θ [°]
29343	10899.69	0.38	66.19	29.83	291.47	68.53
29602	9417.10	0.31	39.88	159.33	96.16	263.81

Table 1 – Initial Keplerian orbital elements for the studied HAMR objects.

The initial Keplerian elements were obtained from the corresponding Two Line Elements (TLE), as well as other important parameters for the simulations such as the ballistic coefficient B^*. The TLE are a mathematical representation of a satellite's mean orbit (https://www.space-track.org/documentation#/tle) for a specific epoch that is frequently updated.

The ballistic coefficient is obtained directly from the object's TLE, anyhow it is necessary to perform a series of manipulations for later use within the code. By definition, we know that B^* can be expressed as:

$$B^* = \frac{1}{2}\rho_0 C_D \frac{A}{m_S}\,[R_E^{-1}] \tag{6}$$

Here ρ_0 is the atmospheric density at perigee of the orbit, C_D is the drag coefficient, A/m_S is the area-to-mass ratio of the object and B^* is expressed at the TLE in inverted Earth radius R_E units.

For the parameter value A/m_S, necessary in the formulation of the PRS, we used the value of B^* and adopted an average value of C_D depending on the height [6]. The area-to-mass ratio found for the studied objects are between 0.1-0.4 m^2/kg.

4. Results

We have simulated the orbital evolution of the two space objects identified by the NORAD numbers 29343 and 29602.

Making use of the initial conditions on Table 1 plus some additional parameters as the specular reflectivity coefficient ($\rho_S = 0.88$) and the aerodynamic drag coefficient ($C_D = 1.8$), propagation was performed for 29343 object from September 4, 2010, 8:32:0.015 UT, the TLE's epoch. The specular reflectivity coefficient and the mean aerodynamic drag coefficient were chosen by the best fit after a series of orbital dynamics simulations on different reasonable values for this kind of object.

The results are in Figure 2, where we can see the variation of the orbital elements until reentry. Secular behavior can be observed with small variations of long period at perigee argument ω, inclination i, and node Ω, while the semimajor axis a and the eccentricity e have a similar behavior until the object enters more deeply inside the atmosphere and these parameters show to be affected more strongly.

In Figure 2 we can see that the ascending node rotates in prograde direction with a rate of change $d\Omega/dt \approx 0.00016506$ [rev/day], while the argument of perigee has a quasi-linear retrograde movement with time variation of $d\omega/dt \approx -0.00097683$ [rev/day], except for the

last five days, where we can see the emergence of a disturbing short component with divergent character. It is further noticed that the orbital inclination decreases very gently with velocity $di/dt \approx -0.000054419$ [rev/day].

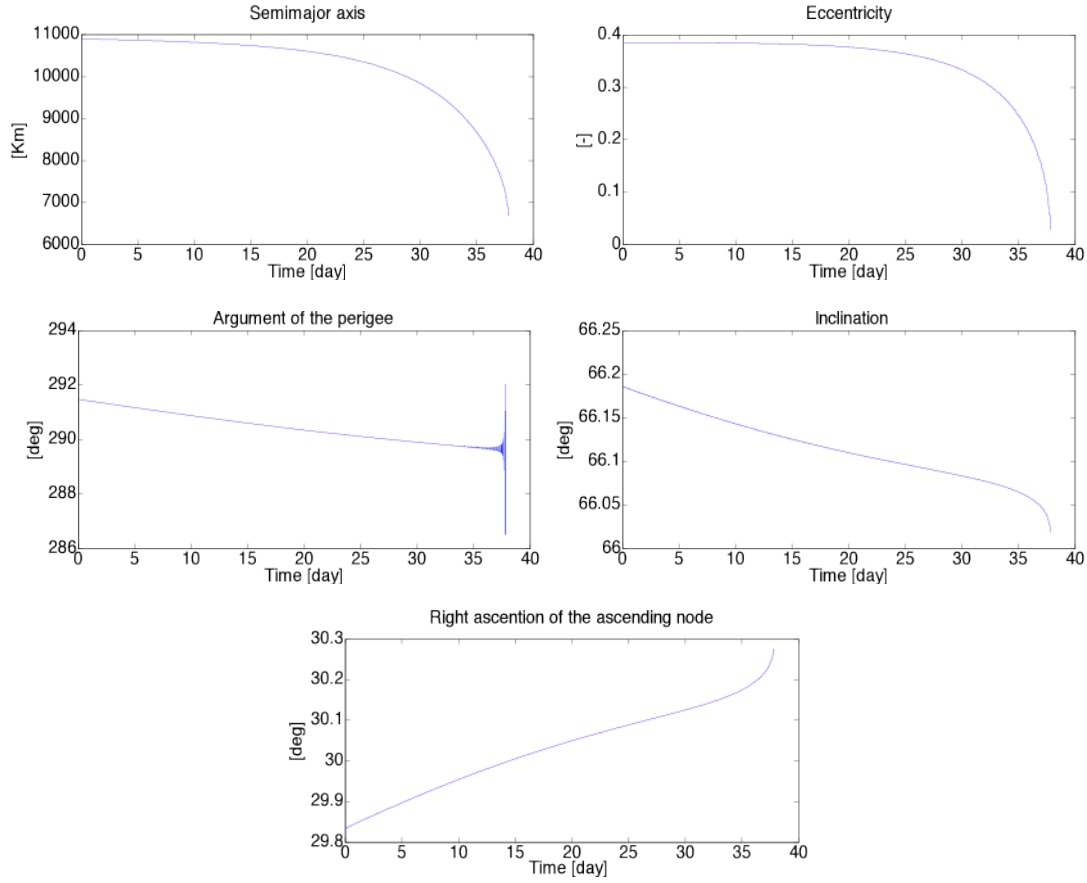

Fig. 2 – Keplerian orbital elements of HAMR 29343 considering SRP and drag effects.

Another significant result can be noticed in Figure 2 and that is the object re-enters after 30.84 days from the initial date, which means that it occurs around October 12, 2010.

For the second object is was made an orbit propagation of the initial parameters according to Table 1 together with the values of specular reflectivity coefficient and drag coefficient average, $\rho_S = 0.21$, $C_D = 1.8$ respectively. Those were chosen with the same kind of simulations performed for the 29343 object. The TLE data epoch used for initialization of the 29602 object trajectory was September 26, 2010 at 23:03:0.495 UT.

The results for 29602 are presented in Figure 3, in which we can see the variation of the orbital elements until re-entry. Secular behavior can be observed with long-period components in the argument of perigee and right ascension of the ascending node. While the semimajor axis, the eccentricity and the inclination, all decrease monotonically, only noticing the atmosphere as moving closer to the Earth's surface and so being strongly affected by the aerodynamic drag force.

Figure 3 shows the ascending node prograde movement of this HAMR object, while the argument of perigee has a smooth variation, except in the last 20 days, when we can see the emergence of a disturbance component with divergent character. It is further noted that the orbital inclination decreases with an approximately constant rate until days before reentry when the rate of decay significantly increases.

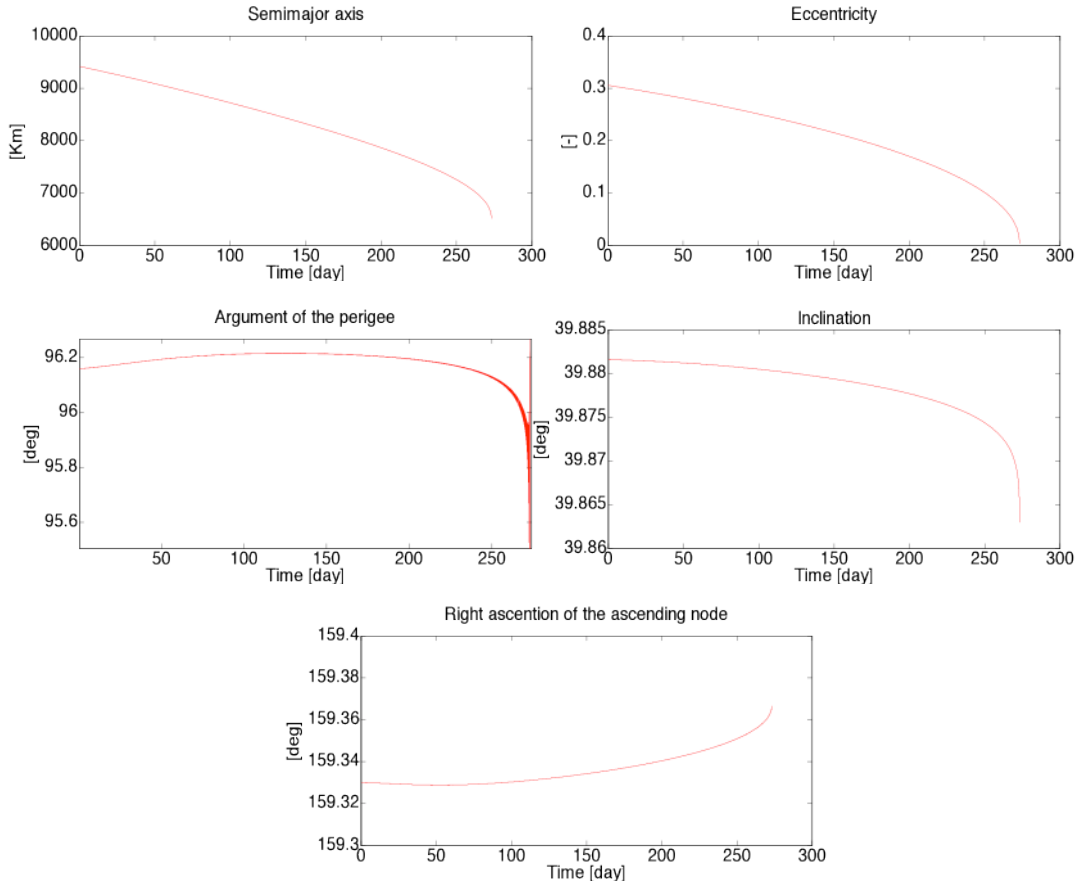

Fig. 3 – Keplerian orbital elements of HAMR 29602 considering SRP and drag effects.

It is also possible to observe in Figure 3 that the object re-enters after 273.2 days from the initial date, which means that it occurs around June 27, 2011. Table 2 summarizes the results relative to the decay time.

NORAD Number	Real decay date	Simulated decay date
29343	October 10, 2010	October 12, 2010
29602	June 21, 2011	June 27, 2011

Table 2 – Real and simulated decay date for the studied HAMR objects.

5. Conclusions

From the results obtained for the two previous cases we may remark that all Keplerian elements behave roughly similarly. As regards the ascending node, its behavior was clearly observed as prograde in both cases with variation rates of the order of 10^{-4} - 10^{-6} [rev/day].

It is possible to notice that the argument of perigee has a smooth retrograde movement in the first case and in the days before reentry, in both cases, a divergent character appears, which can be interpreted as an effect caused by the interaction of the HAMR object with the atmosphere.

As regards the eccentricity, it is noteworthy that the decay observed is the product of the aerobraking effect over the HAMR object that can be interpreted as an orbit circularization. This is a common effect over initially eccentric orbits under the atmospheric drag influence. Furthermore the observed variation in the orbital inclination is caused by the solar radiation

pressure experienced during the entire HAMR orbit, because that is the only force that has components outside the orbital plane.

Finally it is important to remark that for the 29343 object the actual re-entry date was October 10, 2010, while for the 29602 object it was June 21, 2011. Comparing the dates obtained by simulated re-entry trajectories with the real ones, as in Table 2, it can be seen that they only differ in 2 days and 6 days respectively, under simulations of around 30 days in the first case, and almost 9 months in the second one. The difference between the decay dates obtained may possibly be due to the simplified models for representing the disturbance forces, as well as not considering the totality of the external forces to which the HAMR objects are subjected. Additionally we should point the fact that we had to estimate and average the values of some important parameters as the drag coefficient and the specular reflectivity coefficient over the trajectories.

For future research we expect to obtain even better results considering the effects of the Earth's non-homogeneous potential. It is also expected that performing re-entry trajectories simulations for a great variety of HAMR objects can lead us to an analytical expression for defining aerodynamic parameters such as the drag coefficient and the specular reflectivity coefficient.

References

[1] Schildknecht T *et al* 2004 Optical observation of space debris in GEO and in hightly-eccentric orbits *Advances in Space Research* **34**
[2] Schildknecht T *et al* 2008 Properties of the high area-to-mass ratio space debris population at high altitudes *Advances in Space Research* **41**
[3] Scheeres D 2007 The dynamical evolution of uniformly rotating asteroids subject to YORP *Icarus* **188**
[4] Scheeres D *et al* 2011 The dynamics of high area-to-mass ratio objects in Earth orbit: the effect of solar radiation pressure *AAS* 11-178
[5] Montenbruck O and Gill E 2001 *Satellite Orbits. Models, Methods and applications* (Berlin: Springer)
[6] King-Hele D 1987 *Satellite Orbits in an Atmosphere: Theory and Applications* (Glasgow: Blakie)